Electromagnetic Mass and Efficiency of Magnetic Gears for Electrified Aircraft

Thomas F. Tallerico[1] Dr. Justin J. Scheidler [1] and Zachary A. Cameron[1]
NASA Glenn Research Center, Cleveland, Ohio, 44135, U.S.A.

Magnetic gears are currently being developed for use in a variety of industries such as wind and automotive, because of their higher reliability and lower maintenance cost than their mechanical counterparts. The bulk of magnetic gear development to date has focused on maximizing the technology's volumetric torque density (torque per unit volume). In contrast, the primary performance metrics for an aircraft's gear box are its mass and efficiency. To that end, this paper presents a study of the achievable electromagnetic specific torque (torque per unit electromagnetic mass) and efficiency of concentric magnetic gears. NASA's second magnetic gear prototype is used as the baseline for this study. Achievable electromagnetic specific torque and efficiency trends are presented with respect to higher-level design variables such as gear ratio and radius.

I. Nomenclature

ag	=	mechanical airgap size	t	=	time
B	=	magnetic flux density	T	=	time period of magnetic flux repetition
D	=	rotor diameter	TRM	=	total number of ring gear magnets
GR	=	gear ratio	TSM	=	total number of sun gear magnets
l	=	magnet axial lamination thickness	w	=	magnet width
k_1	=	modified Stienmentz coefficient	V	=	magnet volume
M	=	iron mass	α	=	Stienmetz frequency coefficient
MR	=	magnets per ring gear pole pair	β	=	Stienmetz flux density coefficient
MS	=	magnets per sun gear pole pair	ρ	=	resistivity of magnet material
Q	=	number of pole pieces			
PR	=	number of ring gear pole pairs			
PS	=	number of sun gear pole pairs			

II.   Introduction

The use of a gearbox to connect an electric machine to a propeller in an electrified aircraft drive has been shown to provide significant weight savings (Ref 1). These weight savings result from reductions in electric motor weight with reduced output torque. Additionally, increasing electric motor tip speed can also improve an electric motor's efficiency (Ref 1-3). However, mechanically-geared drive systems have significantly lower reliability than direct drive systems, because of the large number of potential failure modes in mechanical gearboxes (Ref 4-5). Most of mechanical gearboxes' wear and failure modes directly result from mechanical gears transmitting torque through tooth contact. In contrast, magnetic gearboxes transmit torque with magnetic fields. They, therefore, have none of the tooth contact related failure modes that exist in mechanical gearboxes and the potential to enable geared electrified aircraft drives with similar reliability to direct drive systems.

Magnetic gears have been explored extensively in recent years for use in wind energy, automotive, and marine energy applications, because of their reliability advantages over mechanical gears (Ref 5-10). The bulk of this exploration has focused on magnetic gear volumetric torque density (torque per unit volume). In contrast, the primary performance metrics for electrified aircraft drive systems are mass and efficiency (Ref 11-12). To that end, NASA began a program in 2016 to assess the potential of magnetic gears to achieve similar mass and efficiency to aerospace-grade mechanical gearboxes (Ref 13-16).

NASA's second prototype magnetic gear (PT-2), seen in Figure 1, currently is the highest specific torque (torque per unit mass) magnetic gear in the open literature. In this paper, the design of PT-2 is used as the baseline for a study

---

[1] Aerospace Research Engineer, Rotating and Drives Systems Branch.

of concentric magnetic gear's achievable specific torque (torque per unit mass) and efficiency. Electromagnetic specific torque and efficiency trends for concentric magnetic gears are presented with respect to higher-level magnetic gear design variables such as gear ratio and radius. Work by Texas A&M University (Ref 17-19) represent the only known similar studies of concentric magnetic gears' potential specific torque and efficiency. Their studies, however, did not explore gears designed with Halbach arrays, which have been shown to improve magnetic gear specific torque (Ref 20). Their studies also assumed a minimum modulator radial thicknesses two times larger than what was achieved in NASA's second prototype. As discussed in References 13-16, Modulator radial thickness is one of the main drivers of a magnetic gear's specific torque. Additionally, their study was conducted for grade N42 neodymium magnets, most likely to limit cost. Higher grade neodymium magnets are more practical for aerospace applications because cost is less of a factor. Grade N52 neodymium is considered in this study, because it was the magnet grade used in PT-2.

Figure 1 NASA's second prototype magnetic gear (PT-2)

In Section III of this paper, a brief description of concentric magnetic gears is provided. Section IV explains the methodology used in the specific torque and efficiency studies presented in this paper. Sections V-IX discuss magnetic gear efficiency and specific torque with respect to magnets per ring gear pole pair (MR), magnets per sun gear pole pair (MS), number of sun gear pole pairs (PS), gear ratio, and radius. Section X provides a discussion of the trends between concentric magnetic gear mass and efficiency.

III.   Concentric Magnetic Gears

The concept of the concentric magnetic gear (CMG) was first proposed in 2004 (Ref 21). A concentric magnetic gear consists of three concentric rotors: a sun gear, a modulator, and a ring gear. An axial cross-section of a CMG is depicted in Figure 2. The sun gear of a CMG is a low-pole-count permanent magnet rotor that is typically used as the high-speed input to the CMG. The ring gear is a high-pole-count permanent magnet rotor. It can either be held fixed or used as the output of the CMG, similar to the ring gear of a mechanical planetary gearbox. The modulator sits concentrically between the ring and sun gear. It consists of alternating sections of high permeability magnetic material (pole pieces) and low magnetic permeability material (typically non-conductive mechanical support structure). The modulator, like the ring gear can either be used as the output of the CMG or held fixed. Kinematically, it behaves similarly to the planet gears of a mechanical planetary gear box.

In order for torque to be transmitted continuously between two magnetic rotors, the rotors typically have to produce magnetic flux with matching spatial harmonic order in the airgaps between the rotors. When the number of pole pieces in the modulator (Q), sun gear magnetic pole pairs (PS), and ring gear magnetic pole pairs (PR) are selected correctly with respect to one another, the modulator spatially modulates the flux produced by the sun and ring gear so that they have matching spatial harmonic order in the CMG's two magnetic airgaps. With matching spatial harmonic order in the two airgaps, torque can be transmitted continuously between all three rotors. The required relationship between the pole counts of the three rotors is given by

$$Q = PR \pm PS \tag{1}$$

References 13-14 provide a detailed explanation of flux modulation in magnetic gears.
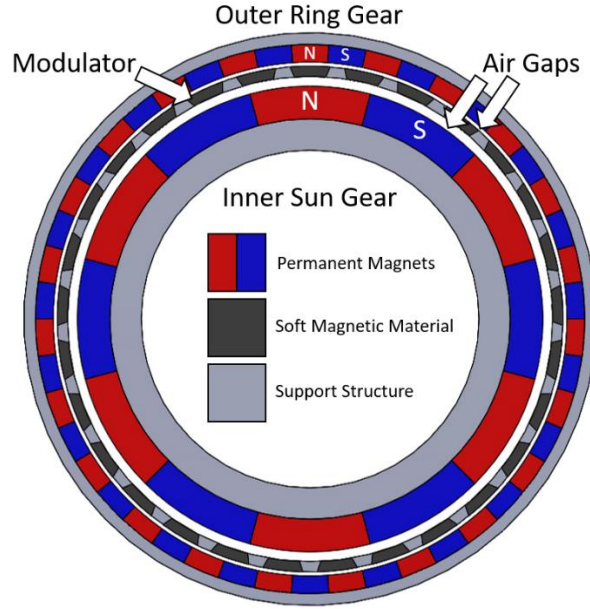
Figure 2 Cross-sectional geometry of a simple concentric magnetic gear

In this paper, the number of pole pieces is assumed to be equal to the number of ring gear pole pairs plus the number of sun gear pole pairs. The ring gear is assumed to be fixed and the modulator is used as the output of the CMG. In this configuration, the gear ratio is given by

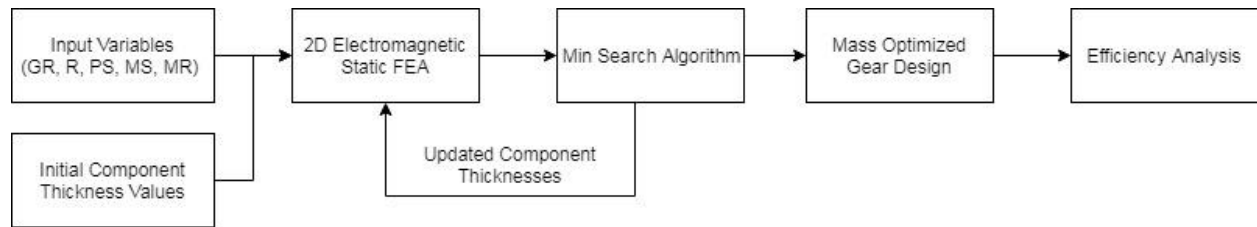$$GR = \frac{Q}{PS} = \frac{PR}{PS} + 1 \qquad (2)$$

IV. Study Methodology

Figure 3 Flow Diagram of Study Methodology

A schematic of the methodology used in this study is presented in Figure 3. In this study, electromagnetic-mass-optimized gear designs are produced for a set of selected higher-level input parameters (MR, MS, PS, gear ratio, and radius) in order to explore the dependence of specific torque on those parameters. An efficiency simulation is then run on most of the mass-optimized gear designs to explore efficiency trends with respect to those same parameters. To ensure that all of the produced designs and the subsequent efficiency simulations are meaningful, PT-2's design was used as the basis and validation point for all the study.

PT-2 was an optimization and scaling of NASA's first magnetic prototype (Ref 13), which was designed for NASA's X-57 Maxwell aircraft's high lift propellers. Details on PT-2's design can be found in references 13-16. In this study, every gear is designed to have the same torque as PT-2 (185 Nm), as quantified by a 2D finite element simulation. 2D simulation torque is typically lower than the torque of a physical CMG prototype because 3D leakage effects are neglected (Ref 27). However, 2D finite element simulations are used for computational speed in the mass optimization, and the actual torque used in the efficiency simulations is assumed to be the experimental pull-out torque of PT-2 (120 Nm). All of the gear designs also have the same output speed (4000 RPM), modulator thickness limitations (2.5 mm), and minimum magnet thicknesses as was used in the design of PT-2. The same magnetic outer radius and mechanical airgap size as PT-2 is also used for all studies except for the study of radius itself. Table 1, lists the assumptions used throughout these studies unless otherwise noted.

Table 1 Design parameters held constant throughout the study and their assumed values unless otherwise noted.

Parameter	Metric	English
Outer Diameter	140 mm	5.51 in
2D Output Torque	185 Nm	1637 in lbf
3D Output Torque	120 Nm	1062 in lbf
Output Speed	4000 RPM	
Mechanical Airgap Thickness	1 mm	0.0394 in
Min Sun Magnet Thickness	5 mm	0.197 in
Min Pole Piece Thickness	2.5 mm	0.0984 in
Min Ring Magnet Thickness	3 mm	0.118 in
Thickness of Walls Between Magnets	0.5 mm	0.0197 in
Inner Pole Piece Span Angle (rad)	$1.2*\pi/PR$	
Mid Pole Piece Span Angle (rad)	$1.2*\pi/PR$	
Outer Pole Piece Span Angle (rad)	$.6*\pi/PR$	
Magnetic Material	Neodymium N52	
Electrical Steel	$Fe_{49}Co_{49}V_2$	
Density of Magnets	7500 kg/m^3	0.271 lb/in^3
Density of Pole Pieces	8000 kg/m^3	0.289 ln/in^3
Allowable Stress in Carbon Fiber	600 MPa	87 ksi

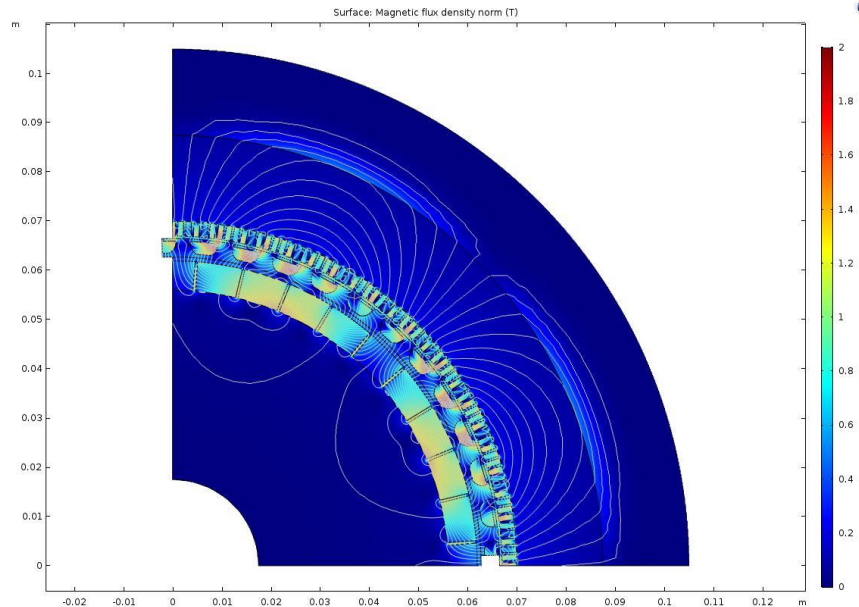## A. Specific Torque Optimized Gear Design Methodology

Figure 4 Magnetic flux density result from a representative 2D electromagnetic finite element simulation used in this study

To create the electromagnetic-mass-optimized gear designs, a 2D electromagnetic finite element simulation of CMG's cross-section spanning a single sun gear pole pair is used (Figure 4). Symmetry of the ring and modulator about a

single sun gear pole pair is enabled through the use of integer gear ratios. This symmetry was inforced for computational efficiency. In actual CMG prototypes, integer gear ratios should be avoided because the symmetry they create leads to a large amount of cogging torque and torque ripple (Ref 22-23). A minimum search algorithm is used to optimize the sun gear magnet, pole piece, and ring gear magnet thicknesses to maximize specific torque. Definitions of these thicknesses are shown in Figure 5.

The definitions of the three span angles used to create the pole piece geometry used in this study are depicted in Figure 5. The values of the angles used are listed in Table 1 and the resulting pole piece geometry is shown in Figure 4. The pole piece geometry used in this study is not recommended for actual magnetic gear design, because it does not enable a mechanical interlock between the pole pieces and their neighboring support posts in the modulator structure. The geometry, however, was found to scale well with changes in the higher-level variables, and it gives close to the same specific torque result that an optimized, mechanically-interlocking pole piece geometry would.
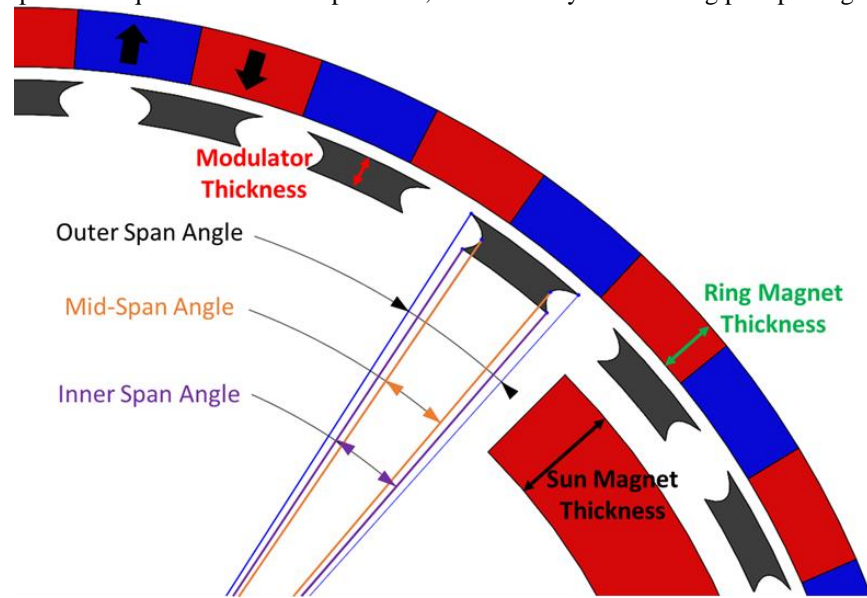

Figure 5 Definitions of pole piece span angles and component thicknesses used.

Two mechanical design considerations were accounted for in each gear design: a half millimeter wall between all magnets and a carbon fiber hoop to retain the high-speed sun gear magnets. PT-2's sun gear with both of these mechanical considerations included is shown in Figure 6. The half millimeter wall is assumed for Halbach array assembly considerations and to avoid being dependent on epoxy bonds for transmitting torque from the magnets to the structure. The half millimeter size is based on the minimum wall size that can be printed by the 3D printers used to produce PT-2's structure The required thickness of the carbon fiber hoop needed to retain the sun gear magnets during high speed rotation was calculated using analytical centripetal loading and hoop stress equations. A conservative maximum allowable stress of 600MPa was assumed for the carbon fiber hoop. The calculated required thickness of the hoop was added to the assumed mechanical airgap between the sun and modulator rotors to set the sun-to-modulator magnetic gap in the 2D FEA electromagnetic simulations.

Figure 6 Sun gear of PT-2 with its carbon fiber magnet retaining hoop and 0.5 mm walls between magnets.

B. Efficiency Analysis Methodology

Efficiency analysis was carried out on the majority of the specific-torque-optimized magnetic gears produced in the specific torque studies. The use of integer gear ratios in the gear designs also reduced computational cost for the efficiency analysis, because the symmetry of the gears made the period of repetition for magnetic flux in the gear equivalent to a sun gear rotation of one sun gear pole pair span angle. To reduce computational efficiency further, rather than simulate the combined electromagnetic response of each gear using a time dependent simulation, this study used a set of static simulations spread uniformly over the operating positions that span the period of repetition. Magnetic flux density as a function of sun gear rotation data was extracted from the collection of static simulations for all the magnetic components of the gear. The flux density vs sun gear rotation data was then post-processed to predict the magnet eddy current and pole piece iron losses in the magnetic gear. With this approach the losses in the gear are approximated, because the eddy currents in the magnetic components do not affect the magnetic field values in the simulations (bidirectional electromagnetic coupling is neglected).

The equation for the eddy current loss in the magnets (Ref 24) used in this study is

$$P_c = \frac{1}{16} \frac{V}{\rho} \frac{w^2 l^2}{w^2 + l^2} \frac{1}{T} \int_0^T (\frac{dB}{dt})^2 \, dt \qquad (3)$$

Where P_c is the power loss in the magnets due to eddy currents, V is the volume of a single magnet, ρ is the resistivity of the magnet material, w is the width of the magnet, l is the length of the axial magnet laminations, T is the period of repetition for the magnetic field, B is the magnetic flux density, and t is time. In this paper, results are presented either assuming the individual magnets in both the sun and ring gears are one solid piece (un-laminated), or that they are made up of 2 mm axial segments of magnet bonded together with non-conductive epoxy to the length of the gear. In the case of the magnets being one solid piece, l in Equation 3 is equal to L, the active axial length of the gear. In the case of the 2 mm axial segments, hence forth referred to as 2 mm magnet laminations, l is equal to 2 mm. Both cases are presented, because NASA has found, as will be shown in this paper, that the use of magnetic laminations can enable magnetic gears to have electromagnetic efficiencies greater than 99%. The 2 mm lamination size was selected for this study based on experience with magnet manufacturers and the difficulties they had when producing laminations smaller than 2 mm.

The iron/modulator loss model used in this study is the improved generalized Stienmetz equation (Ref 25):

$$P_c = \frac{M}{T} \int_0^T k_1 \left| \frac{dB}{dt} \right|^\alpha (\Delta B)^{\beta - \alpha} dt \qquad (4)$$

Where P_v is the power loss in the iron, M is the mass of iron, ΔB is the peak-to-peak flux density, and $k_1, \alpha,$ and β are coefficients based on material testing data from the material's manufacturer. This model is used because it has the capability to deal with minor loops in the flux density of iron components. Minor loops are common in the magnetic response of a magnetic gear's pole pieces because of the two different pole count permanent magnet rotors producing flux in the pole pieces. Details on the implementation of the iron and magnet loss models are provided in the Appendix.

V. Effect of Magnets per Ring Gear Pole Pair (MR)

MR and MS are included in this study to show separately the effects of total ring magnet count (TRM) and total sun magnet count (TSM) on magnetic gear specific torque and efficiency independent of sun and ring gear pole count changes. For the study of MR an outer radius of 7 cm and a gear ratio of 4 was used similar to PT-2. MS was set to 10. Parametric sweeps of PS and MR were performed and mass optimized gear designs were produced for each combination. Table 2 lists the higher-level variable values used in this study.

Table 2 Higher-level variable values for MR study

MR Study Parameters	
Radius	7 cm
Gear Ratio	4
Sun Gear Pole Pairs (PS)	4, 6, 8, 10, 12
Magnets per Sun Gear Pole Pair (MS)	10
Magnets per Ring Gear Pole Pair (MR)	4, 6, 8, 10

A. Achievable 2D Electromagnetic Specific Torque

The variation of achievable 2D electromagnetic specific torque with MR is shown in Figure 7. The trends in Figure 7 result from two competing effects of increased MR: the fact that the specific flux of Halbach arrays increases with increased magnet per pole count (Ref 13) and the loss of ring gear magnet fill percentage due to this study's assumption of a 0.5 mm wall between magnets.
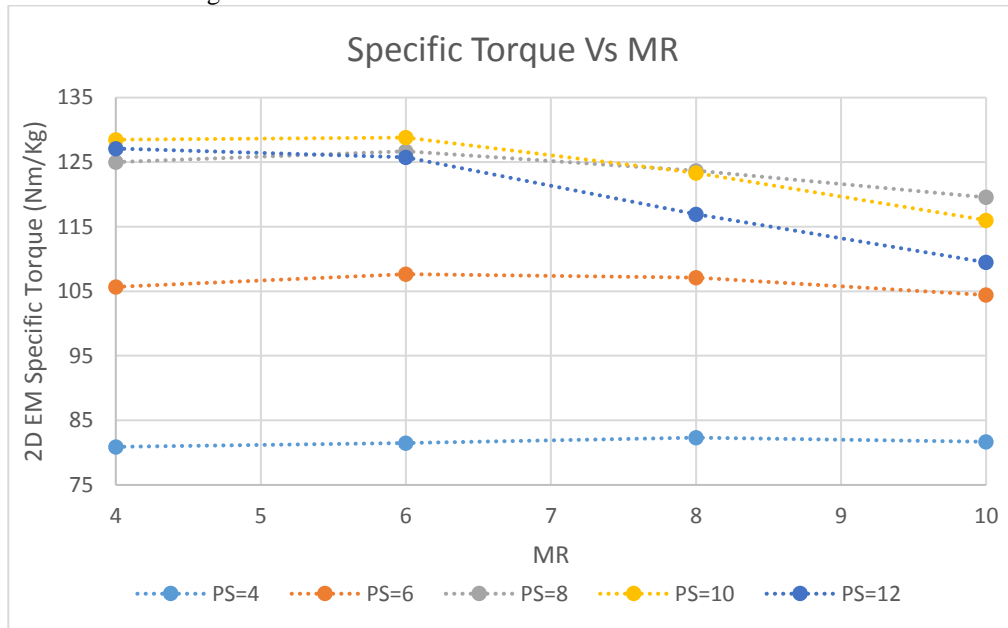

Figure 7 Specific torque variation with respect to MR

The assumed 0.5 mm wall between magnets results in a loss of ring gear magnet fill percentage in the circumferential direction as the total ring magnet count increases. Total ring magnet count is defined by

$$TRM = PR * MR = (GR - 1) * PS * MR \tag{5}$$

The loss of ring gear magnet fill percentage as TRM increases is shown in Figure 8a. The variation of TRM for the values of PS and MR used in this study is shown in Figure 8b. In the absence of the increase in Halbach array specific flux with increased magnet per pole count, the loss of in plane magnet fill percentage that results from increasing MR reduces the torque produced per axial length in a magnetic gear. Correspondingly in a mass optimized gear design, as

in plane ring gear magnet fill percentage is reduced, the magnetic gear's axial length gets longer and the overall mass of the gear increases.

At low values of PS, the slope of TRM with respect to MR is lower, and the loss of magnet fill percentage is correspondingly less with increased MR. At these low PS values (4 and 6), the increase in Halbach array specific flux with increased MR overrides the loss of magnet fill percentage and specific torque increases slightly with increased MR at low MR values. There are diminishing marginal returns for specific flux improvements with increasing the number of magnets per pole in a Halbach array. Correspondingly, for PS values of 4 and 6, at higher MR values the magnet fill percentage loss becomes the dominant effect of MR increasing and specific torque drops with increased MR.

At higher PS values, the slope of TRM with respect to MR is higher, and loss of magnet fill percentage with increasing MR is more significant. At these PS values (10 and 12), the increase in array specific flux with increasing MR never outweighs the effect of the magnet fill percentage loss and specific torque always decays.

It should be noted that the results presented here are specific to the gear ratio and radius used in this study. Changes to either of those values will shift the trends of specific torque with respect to MR, but the trends stay the same as long as a 0.5 mm wall between magnets is maintained. In the absence of the 0.5 mm walls (100 % magnet fill percentage), increasing MR would always increase the specific torque of a magnetic gear, but with diminishing marginal returns, corresponding to the diminishing marginal returns of magnets per pole pair count on the specific flux of Halbach arrays.
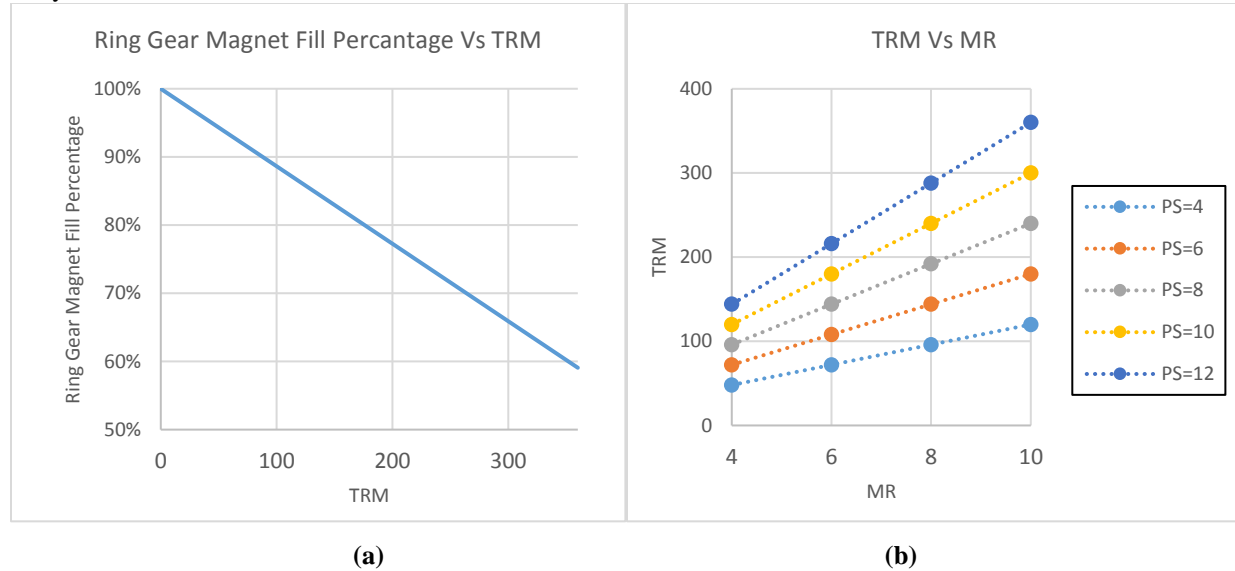

(a)   **(b)**

Figure 8 Effect of total ring magnet count on magnetic fill percentage and variation of total ring magnet count with MR and PS

B. Efficiency without Magnet Laminations

The variation in efficiency and ring gear eddy current loss with increasing MR is shown in Figure 9. For all PS values except for 12, efficiency is shown to always increase with increasing MR in Figure 9a, because of the ring gear loss reduction shown in Figure 9b. In the absence of magnet laminations, magnet width is the smallest length scale for the magnets in the gear designs presented in this paper. Ring gear magnet width varies linearly with TRM and is between 1 and 8 mm for the gear designs in this study. In contrast, axial magnet length is greater than 50 mm for all of the designs. Per Equation 3, when magnet width is much less than magnet length, magnet eddy current loss is proportional to magnet width squared. Correspondingly, in Figure 9b, as MR doubles from a value of 4 to a value of 8, ring gear losses drop by approximately a factor of 4 for all the gear designs in this study.

In Figure 9a, efficiency drops for a PS value of 12 as MR is increased from 8 to 10, due to the increase in gear mass resulting from the reduced 2D specific torque shown in Figure 7. This increased mass results from the additional axial length needed to compensate for the loss of ring gear magnet fill percentage. The additional axial length results in an increase in sun gear magnet losses that cancels out the reduction in ring magnet loss and results in overall lower efficiency.
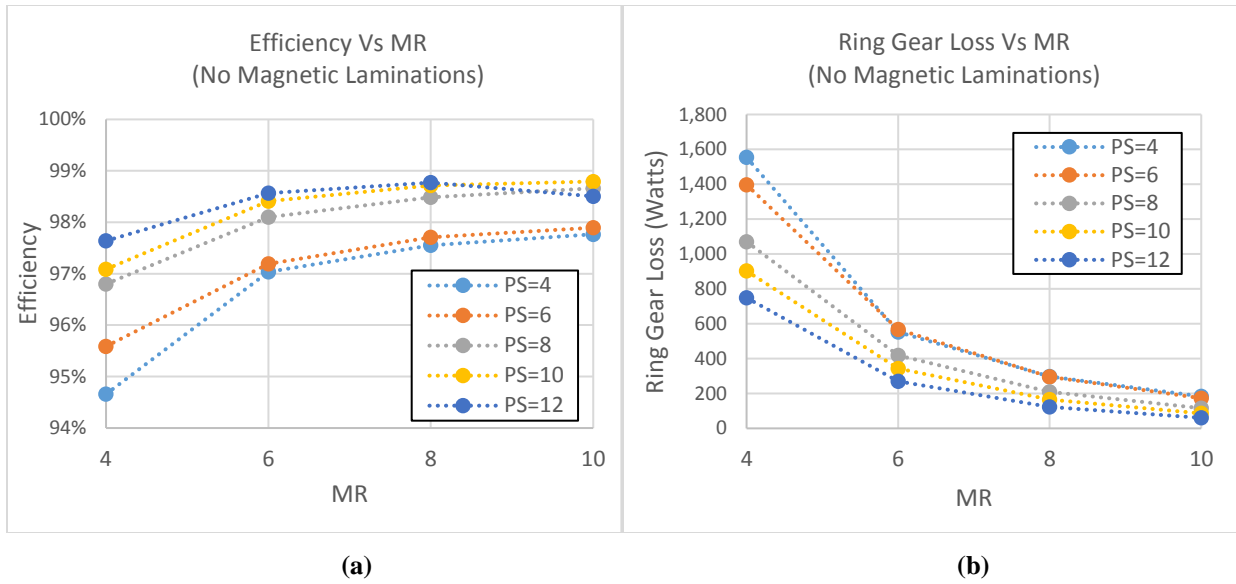
(a)   **(b)**

Figure 9 Effect of MR on magnetic gear efficiency and ring gear losses in the absence of magnet laminations

C. Efficiency with 2mm Magnet Laminations

The effect of MR on magnetic gear efficiency when the magnets are constructed of 2 mm laminations is shown in Figure 10a. The efficiency trends with respect to MR are the same with and without magnet laminations. However, with magnet laminations the variation in efficiency with respect to MR in Figure 10a is between 0.1% and 0.3% whereas it was 1% to 3% without laminations in Figure 9a. As can be seen comparing Figure 10b to Figure 9b, the addition of magnet laminations reduced ring gear loss significantly and therefore the reductions in ring magnet loss with increasing MR are less impactful on gear efficiency.

In Figure 10b, it can also be seen that at lower TRM values (Low PS and MR), MR has a smaller effect on ring gear magnet loss than it does at higher TRM values. This lower effectiveness of MR at lower TRM values, results from the magnet width being greater than the size of the 2 mm magnet laminations. Per Equation 3, when magnet width is significantly greater than the magnet lamination size, magnet width reduction has less of an effect on magnet eddy current losses.
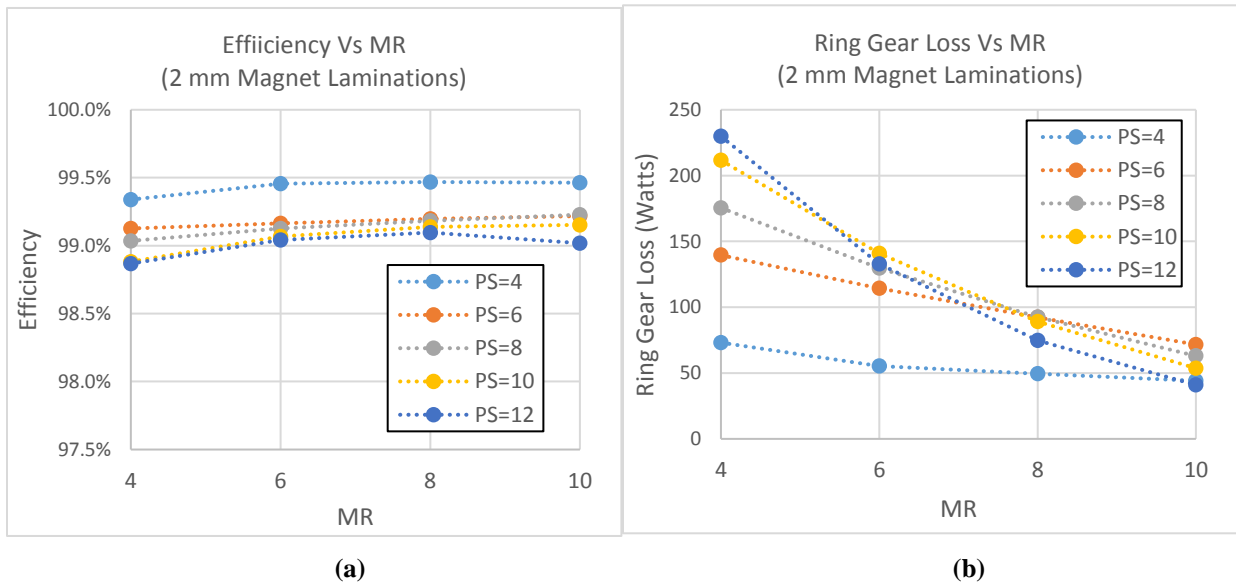

(a)   **(b)**

Figure 10 Effect of MR on magnetic gear efficiency and ring magnet losses when 2 mm magnet laminations are used.

9

Overall, comparing Figure 10a to Figure 9a, the addition of magnet laminations enabled most the gear designs to achieve greater than 99% electromagnetic efficiency. This result is one of the key findings of NASA's magnetic gearing program as these efficiency values are comparable to the efficiencies typically achieved by aerospace grade mechanical gearboxes.

VI. Effect of Magnets per Sun Gear Pole Pair (MS)

For the study of MS, similar to MR a radius of 7 cm and a gear ratio of 4 was assumed. MR was held fixed at 6. Parametric sweeps of PS and MS were performed. Table 3 lists the values of the higher-level variables used in the MS study.

Table 3 Higher-level variable values used in MS study

MS Study Parameters	
Radius	7 cm
Gear Ratio	4
Sun Gear Pole Pairs (PS)	4, 6, 8, 10, 12
Magnets per Sun Gear Pole Pair (MS)	4, 6, 8, 10, 12
Magnets per Ring Gear Pole Pair (MR)	6

A. Achievable 2D Electromagnetic Specific Torque

The effect of MS on achievable specific torque is shown in Figure 11. An initial large increase in specific torque for all PS values is shown in Figure 11 as MS is increased from 4 to 6. This large increase in specific torque results from a large increase in Halbach array specific flux as magnets per pole pair is increased from 4 to 6. Further increase of MS past 6 only varies the specific torque of the gear designs by less than 1 Nm/kg, because of the diminishing marginal returns on increased magnet per pole pair count in a Halbach array.
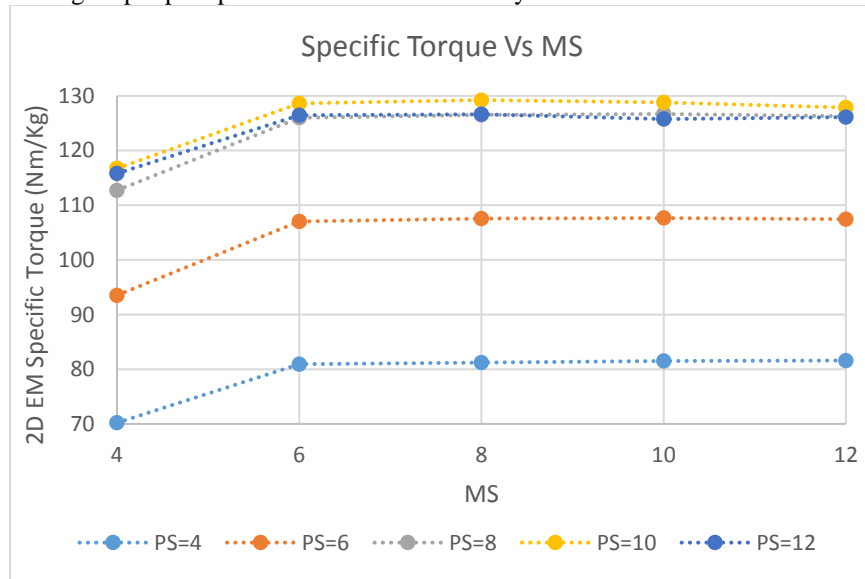

Figure 11 Effect of MS on specific torque

For all PS values, except for a PS value of 4, there is a MS value above which specific torque drops. These drops in specific torque are the result of the 0.5 mm wall assumption and high TSM causing loss of magnetic fill percentage. However, since TSM is defined by

$$TSM = PS * MS \tag{6}$$

the increase in TSM with increased MS is three times less steep than the increase of TRM with MR for the gear ratio assumed in this study. Magnet fill percentage is therefore lost more gradually as MS increases. As a result, no significant loss of specific torque is shown in Figure 11, even at the highest MS and PS values used in this study.

B. Efficiency without Magnet Laminations

The effects of MS on magnetic gear efficiency and sun gear magnet loss in the absence of magnet laminations are shown in Figure 12. Similar to ring gear magnet losses, in the absence of magnet laminations, sun gear magnet losses decrease with approximately the square of sun magnet width which decreases linearly with increased MS. Correspondingly, efficiency increases as MS is increased for all of the gear designs.
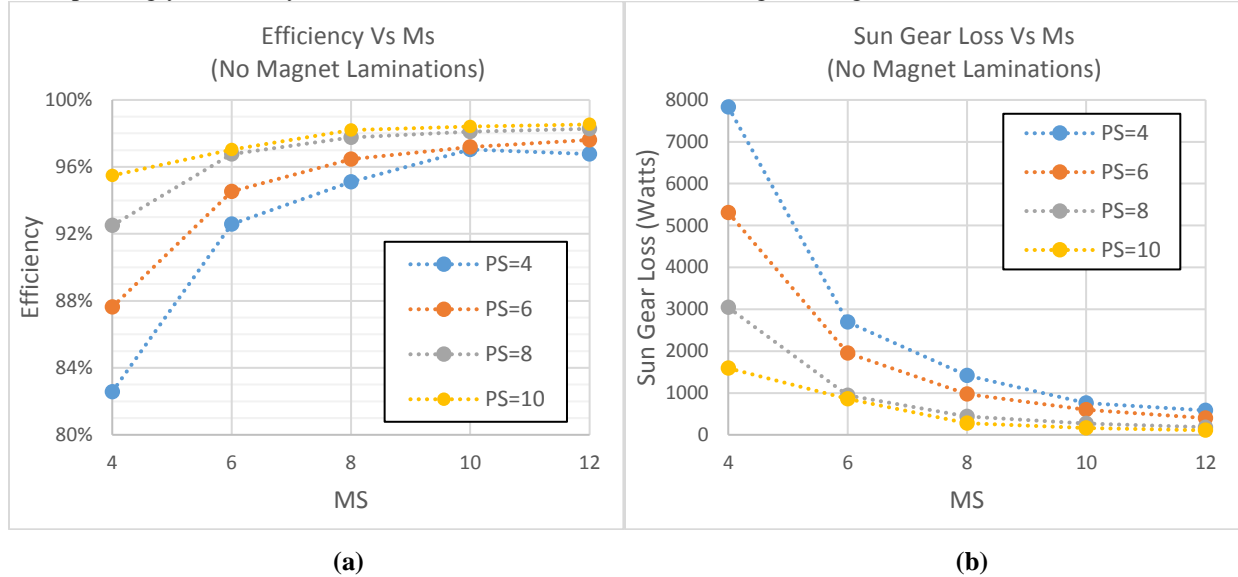

(a)   **(b)**

Figure 12 Effect of MS on magnetic gear efficiency and sun gear losses

Comparing ring gear magnet losses in Figure 9b to sun gear magnet losses in Figure 12b, sun gear magnet losses are shown to be significantly higher. Sun gear magnet losses are higher in these studies for three reasons: TSM is significantly lower than TRM for the parameter values used in this study and correspondingly sun magnet width is much larger than ring magnet width; the sun magnets in all of the designs are approximately two times thicker than the ring gear magnets and therefore have approximately double the volume; and the frequency of the ring gear pole passage on the sun gear at a gear ratio of four is three times the frequency of sun gear pole passage on the ring gear.

C. Efficiency with 2mm Magnet Laminations

The effect of MS on magnetic gear efficiency and sun gear magnet losses with 2 mm magnet laminations is shown in Figure 13. Similar to the variation of efficiency with MR when 2 mm magnetic laminations are used, the variation in efficiency with MS when the magnets are laminated is very small (<0.2 %).
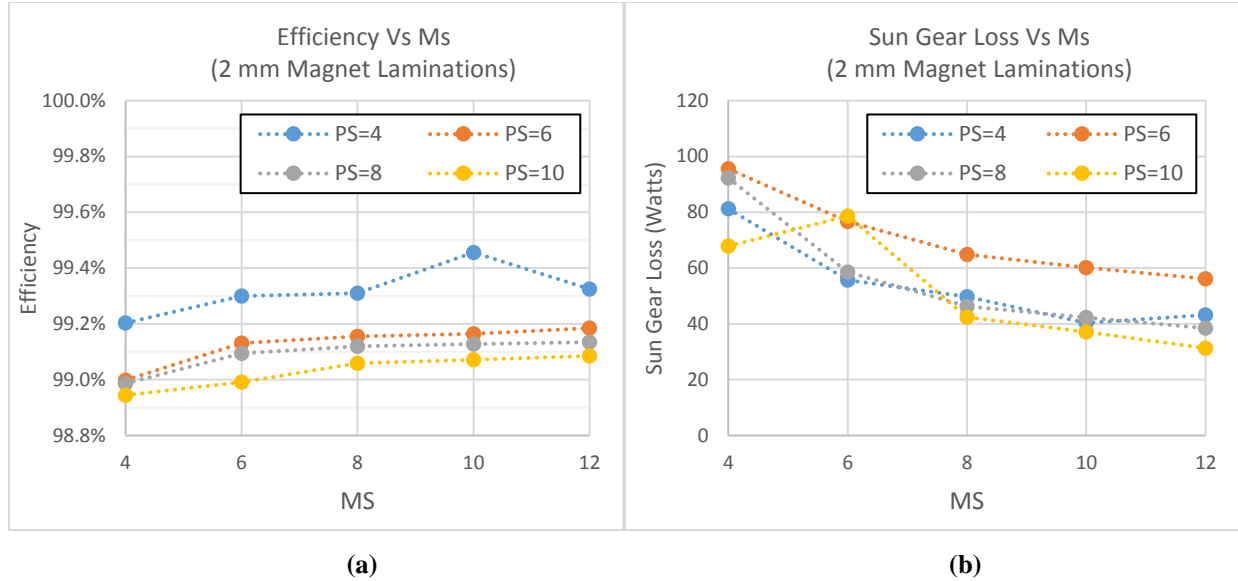
Figure 13 Effect of MS on magnetic gear efficiency and sun gear magnet losses with 2 mm magnet laminations

Comparing Figure 13b to Figure 12b, the effect of MS on sun gear magnet losses are significantly lower in the presence of magnet laminations. Sun gear magnet losses only decrease by less than a factor of 2 when MS is tripled from 4 to 12 for all PS values. The smallest sun magnet width for the gear designs in this study is greater than 2 mm. Correspondingly, per Equation 3, magnet width does not play a significant role in the sun gear magnet eddy current loss generation when the magnets are laminated. The decrease in sun gear loss between an MS of 4 and 6 for all PS values is primarily the result of the mass reduction (specific torque increase) shown in Figure 11.

VII.   Effect of Sun Gear Pole Pair Count (PS)

For the study of PS, an outer radius of 7 cm was again assumed. MS and MR were held fixed at 10 and 6 respectively. 10 and 6 were selected, because they represent high magnet counts that will enable high efficiency without significant magnet fill percentage loss at high PS values. As will be shown, optimum PS value is highly coupled to the gear ratio at a set radius. For this study gear designs were produced for a matrix of gear ratio and PS values. The values of the higher-level parameters used in this study are listed in Table 4.

Table 4 Higher-level Variable Values used in the PS Study

PS Study Parameters	
Radius	7 cm
Gear Ratio	4, 6, 8, 10
Sun Gear Pole Pairs (PS)	4-13
Magnets per Sun Gear Pole Pair (MS)	10
Magnets per Ring Gear Pole Pair (MR)	6

A. Achievable 2D Electromagnetic Specific Torque
The effect of PS on achievable magnetic gear specific torque at various gear ratios is shown in Figure 14. In Figure 14, an interdependence between gear ratio and optimum PS is shown. The interdependence is mostly caused by PS and gear ratio combining to set ring gear pole pair count (PR) via Equation 2. PR value at a set MR value controls two specific torque reducing phenomenon: the TRM effects on the ring gear magnet fill percentage and ring gear pole-to-pole airgap leakage flux percentage.

Ring gear pole-to-pole airgap flux leakage is flux that links between two poles on the ring gear through the airgap rather than crossing the airgap into the modulator. This flux that leaks pole-to-pole on the ring gear does not couple with the sun gear flux and therefore does not produce torque. The percent of the ring gear's flux that leaks pole-to-pole is determined by the relative reluctance of the coupling and leakage flux paths. The reluctance of the coupling path is largely set by the thickness of the CMG's airgaps. The reluctance of the pole-to-pole leakage path is mostly driven by the circumferential distance between poles on the ring gear. The relative ratio of the airgap thickness to the ring gear pole-to-pole distance therefore governs what percent of the ring gear's flux leaks pole-to-pole. At a set radius pole-to-pole distance decreases linearly with increasing PR. Correspondingly ring gear pole-to-pole leakage percentage increases.

By the nature of Equation 2, PR is significantly larger than PS and the ring gear's pole-to-pole distance is shorter than that of the sun gear. As a result, a higher percentage of the ring gear flux leaks pole-to-pole than sun gear flux. Correspondingly, additional magnet material is more effective at producing torque on the sun gear than it would be on the ring gear, because a higher percentage of the added material's flux will be in the coupling path. As a result, the ring gear magnets are typically radially thinner than the sun gear magnets in a mass or volume optimized CMG design.

In the absence of ring gear pole-to-pole leakage and magnet fill percentage effects, specific torque would always increase with increased PS. Increasing PS reduces pole-to-pole distance on the gears' Halbach arrays. Reduced pole-to-pole distance improves array specific flux (Ref 13) and reduces the optimal modulator thickness. Optimal modulator thickness reduces with reduced pole-to-pole distance because the reluctance between poles is smaller and therefore less pole piece thickness is required to significantly affect the reluctance between poles and create flux modulation.
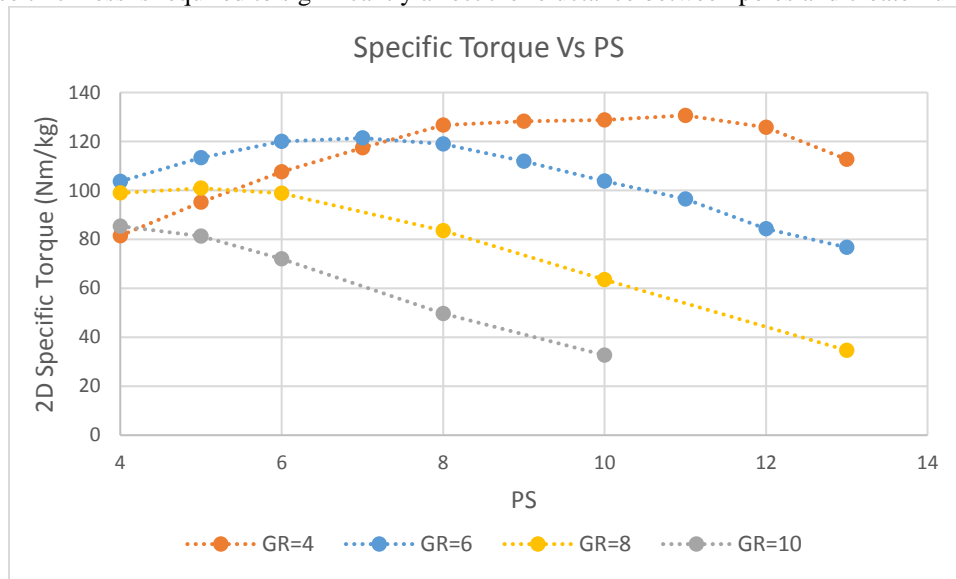

Figure 14 Effect of PS on achievable specific torque at various gear ratios

At low PR values (low PS values and low gear ratios), ring gear pole-to-pole leakage and magnet fill percentage effects are negligible and specific torque increases with increased PS, because the optimal modulator gets thinner and the arrays gain specific flux. This specific torque increase can be seen in Figure 14 for a gear ratio of 4 between PS values of 4 and 8. The specific torque increase is almost linear. At a PS value of 8 and a gear ratio of 4 in Figure 14, the modulator reaches the 2.5 mm minimum modulator thickness limit set for this study. Beyond that point, until a PS of 11, specific torque increase is more marginal because only the improvements to Halbach array specific flux due to reduced pole-to-pole distance contribute to specific torque improvements.

At some point for every gear ratio in this study, increasing PS led to a drop in achievable specific torque. The PS value at which this occurs for each gear ratio corresponds to the modulator thickness being at its minimum value and PR being in the range of 32 to 36 pole pairs. The pole-to-pole distance on the ring gear in this PR value range is around 6 mm. This is the point where ring gear pole-to-pole flux leakage and magnet fill percentage effects become more significant than specific flux gains for the arrays. As a result, specific torque decays with increased PS after this point.

B. Efficiency

The effect of PS on efficiency is shown in Figure 15 both for un-laminated magnets (15a) and laminated magnets (15b). In both cases, increasing PS increases the electrical frequency of the flux produced by the ring and sun gear on the modulator. In both the case of un-laminated and laminated magnet, this increased frequency results in increased modulator loss. In the case of the magnets being laminated, modulator iron losses are the dominate losses in the magnetic gear designs, because the laminations reduce the magnet losses to negligible values. The increasing modulator losses with increased PS, therefore, result in efficiency always decreasing with increased PS value in Figure 15b.

In the case of the magnets being un-laminated, magnet losses dominate and the modulator losses play a minimal role in the efficiency trends of Figure 15a. Increased PS also results in a proportional increase of the electrical frequencies of the sun and ring gears' magnetic flux on one another and a proportional reduction in ring gear and sun gear magnet width. In the ring gear, the magnet width is always much smaller than the magnet length and the effective resistivity of the magnet goes with the width squared. The reduction in ring magnet width, proportional to PS, therefore cancels the effect of the increased sun gear flux electrical frequency. The losses in the ring gear therefore mostly trend with the magnitude of the unmodulated sun gear's flux that reaches its magnets. The magnitude of this flux decays with increased PS as sun gear pole to pole distance gets shorter and ring gear losses decrease almost linearly with increased PS.

In the sun gear, the magnet width is larger and magnet length still plays a significant role in the effective resistance of the magnet to eddy currents. The dependence on magnet length results in sun gear magnet losses trending with the axial length and mass of the gear designs. When the magnets are un-laminated, sun gear magnet losses are the largest losses in the magnetic gear designs of this study. Comparing Figure 15a to Figure 14, the trends of efficiency without magnet laminations and mass with respect to PS are very similar as a result.
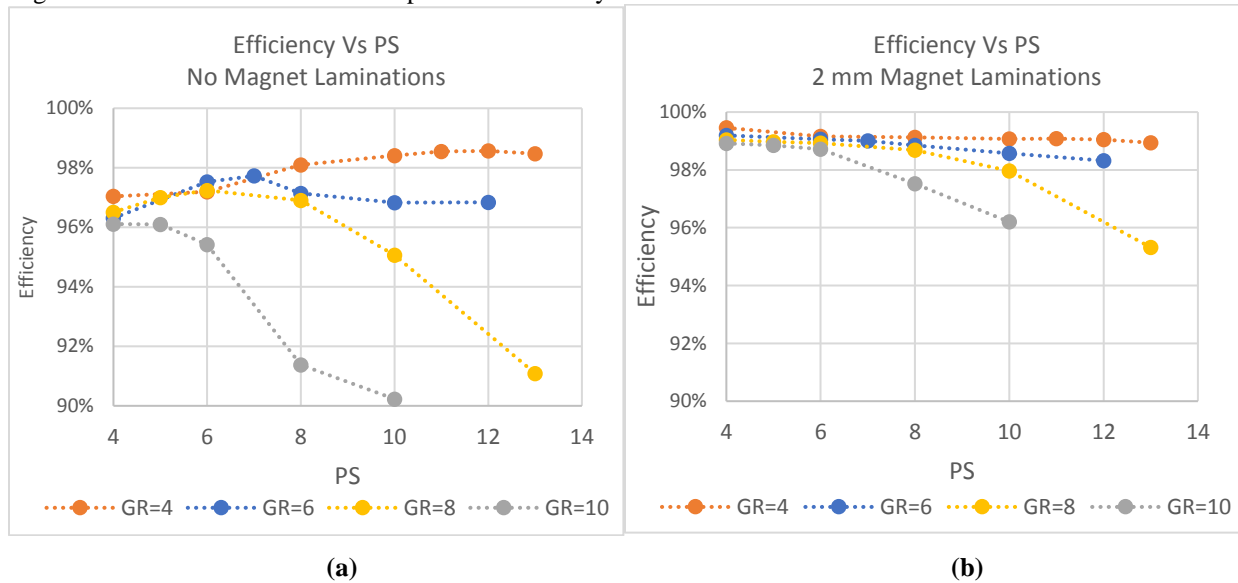

(a)   (b)

Figure 15 Effect of PS on efficiency with and without 2 mm magnet laminations

VIII.   Effect of Gear Ratio

For the study of gear ratio, an outer radius of 7 cm, a MS of 10, and a MR of 6 were assumed similar to the study of PS. Mass optimum gear designs were produced for a matrix of gear ratios and PS values. This section only presents data for a PS value of 6 and the mass optimum PS value for each gear ratio (Figure 16b). The values of the higher-level variables used in this study are listed in table 5.

Table 5 Higher-level Variable Values used in the Gear Ratio Study

Gear Ratio Study Parameters	
Radius	7 cm
Gear Ratio	4-12
Sun Gear Pole Pairs (PS)	4-13
Magnets per Sun Gear Pole Pair (MS)	10
Magnets per Ring Gear Pole Pair (MR)	6

A. Achievable 2D Electromagnetic Specific Torque

The effect of gear ratio on achievable specific torque and the corresponding optimum PS value at a given gear ratio are shown in Figure 16. Specific torque decays almost linearly with gear ratio past a gear ratio value of 5 in Figure 16a. The optimum PS value also decays linearly past a gear ratio of 5, in Figure 16b, until it reaches the minimum PS limit used in this study. The decay in optimum PS corresponds to the value of PS at which PR reaches a value of 32 to 36 dropping as gear ratio is increased per Equation 2. This PR value range corresponds to where ring gear pole-to-pole leakage and magnet fill percentage effects become dominant as was discussed in Section VII-A. It is important to note that with varied radius or airgap size, PR values of 32-36 would not be optimum as the pole-to-pole distances and the relative reluctances of the coupling and leakage paths would change.
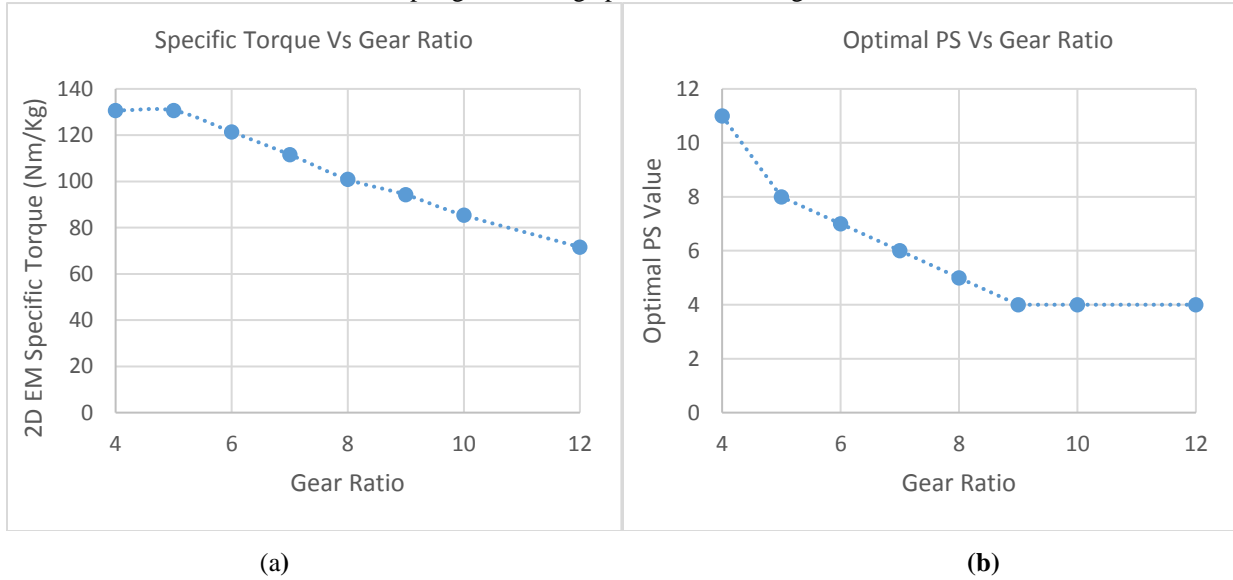

(a) (b)

Figure 16 Effect of gear ratio on achievable specific torque and the corresponding mass-optimum PS Value at a given gear ratio

The bulk of the specific torque reduction seen in Figure 16a is driven by increases in thickness of the sun magnet's carbon fiber retaining hoop. Since output speed was held fixed at 4,000 RPM in this study, increases in gear ratio result in increases to the sun gear's rotational speed. The sun gear's rotational speed increases from a value of 16,000 RPM at a gear ratio of 4 to 40,000 RPM at a gear ratio of 10 in this study. Correspondingly, the required carbon fiber hoop thickness increases from less than 1 mm to 4 mm and the magnetic gap between the sun gear and the modulator increases from less than 2 mm to 5 mm. This large increase in magnetic gap increases the reluctance of the coupling path and leads to reduced specific torque. If a smaller output speed had been used or if input speed had been held fixed rather than output speed, the degradation of specific torque with gear ratio would have been less significant. Reference 19 shows specific torque gear ratio trends for zero output speed.

There is an additional specific torque reduction that results from the decreasing optimum PS in Figure 16. Lower PS values lead to higher pole-to-pole distances for the sun gear Halbach arrays and result in lower magnet specific flux. In this study, this effect is secondary however to the increase in the magnetic airgap size in this study, but it would be more impactful for lower output speeds.
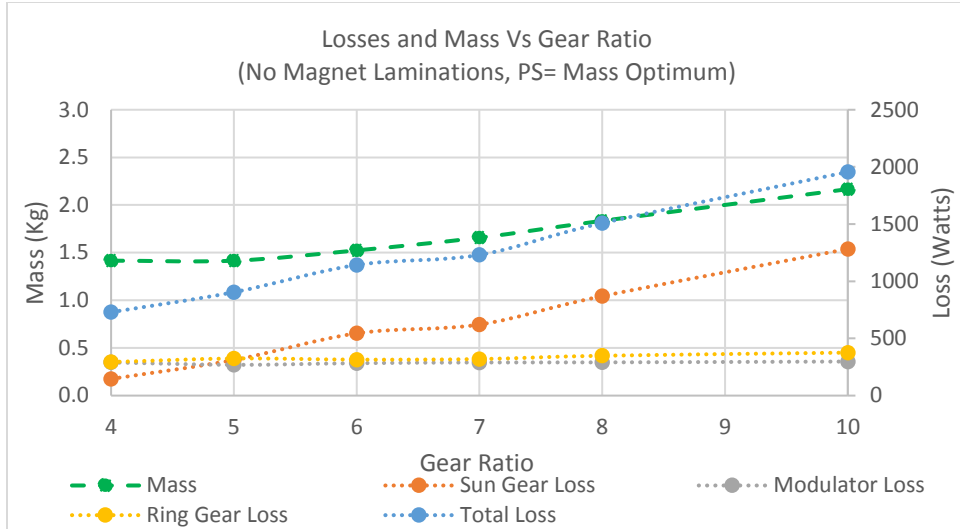
B. Efficiency without Magnet Laminations

The effect of gear ratio on magnetic gear efficiency and losses in the absence of magnet laminations is shown in Figure 17 both at the mass optimum PS (Figure 17b) and a constant PS value of 6 (Figure 17c). Both results at the mass optimum PS and a PS of 6 are presented because different effects cause their efficiency trends.

At the mass optimum PS values, the electrical frequency of the sun gear acting on the ring gear and modulator is around 2500-3000 Hz for all gear ratios. Ring magnet width is also basically the same for all of the designs because the value of PR is roughly the same at 32-36 pole pairs. As a result, ring gear and modulator losses are essentially constant with increasing gear ratio. The sun magnets, on the other hand, increase in width as optimum PS decreases with gear ratio (Figure 16b), because MS is held constant. Additionally, since the speed of the sun gear increases with increased gear ratio and PR is essentially constant (32-36 pole pairs), the electrical frequency of the unmodulated ring gear flux on the sun gear increases. The result is the increasing sun gear magnet losses and the always decreasing efficiency with increased gear ratio shown in Figure 17b.

At a constant PS, the electrical frequency of the sun gear on the ring gear and modulator increases with increased gear ratio, because of the increase in sun gear rotational speed. Modulator losses increase with increased gear ratio as a result. However, ring gear losses are reduced, because at a constant PS, increasing gear ratio increases TRM and reduces the ring gear's magnet width. The sun magnets have essentially a constant width as gear ratio increases at constant PS, but since PR and sun gear rotation speed both increase with increasing gear ratio at constant PS, the electrical frequency of the ring gear on the sun gear increases more significantly with increased gear ratio than it did in the mass-optimum PS case. Additionally, the gear axial length and mass increase more significantly as gear ratio increases at a constant PS, because PR increases above 32-36 pole pairs and correspondingly ring gear pole-to-pole leakage and magnetic fill percentage effects become significant (as detailed ins Section VII A). The result is the more non-linear variation in sun gear magnet losses shown in Figure 17c. Efficiency initially increases with gear ratio, at constant PS of 6, as the gear axial length and mass are reduced, and then it decreases as the ring gear electrical frequency on the sun and the gear mass increase.
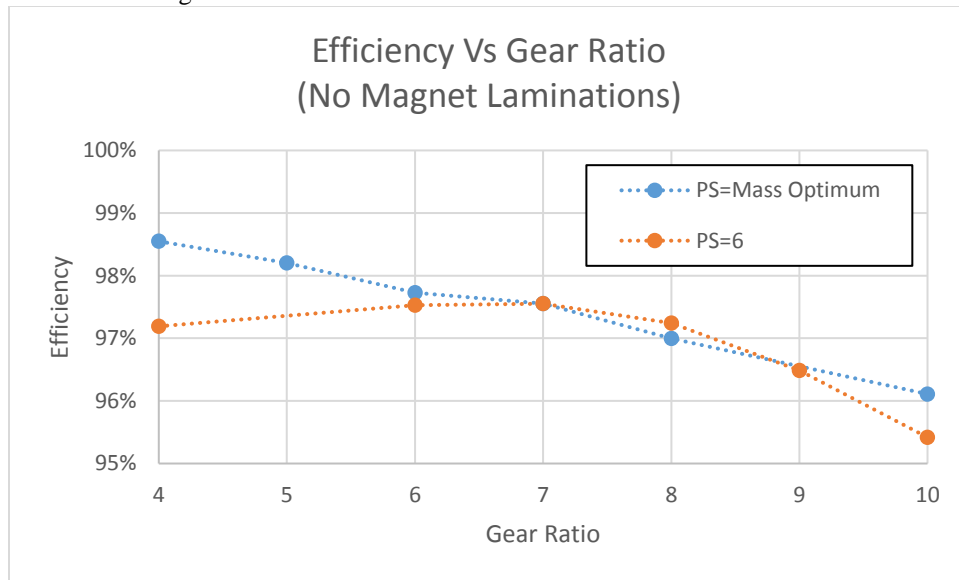
(a)

(b)
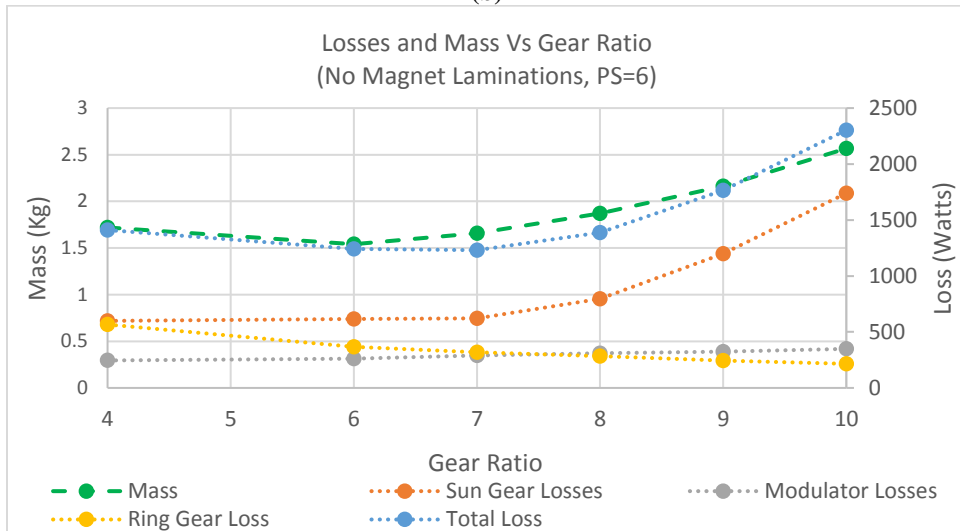
(c)

Figure 17 Effects of gear ratio on magnetic gear efficiency and losses both at a PS of 6 and the mass optimum PS without magnet laminations

C. Efficiency with 2 mm Laminations

The effect of gear ratio on efficiency when 2 mm laminations are used on the sun and ring gear is shown in Figure 18. At the mass-optimum PS, efficiency is almost constant. The small decay shown results from increases in modulator loss resulting from the mass increase (specific torque reduction) with gear ratio shown in Figure 16a. The steeper efficiency reduction with gear ratio observed for a constant PS of 6 results from the increase in the electrical frequencies of the sun and ring gears on the modulator as sun gear speed and PR increase.
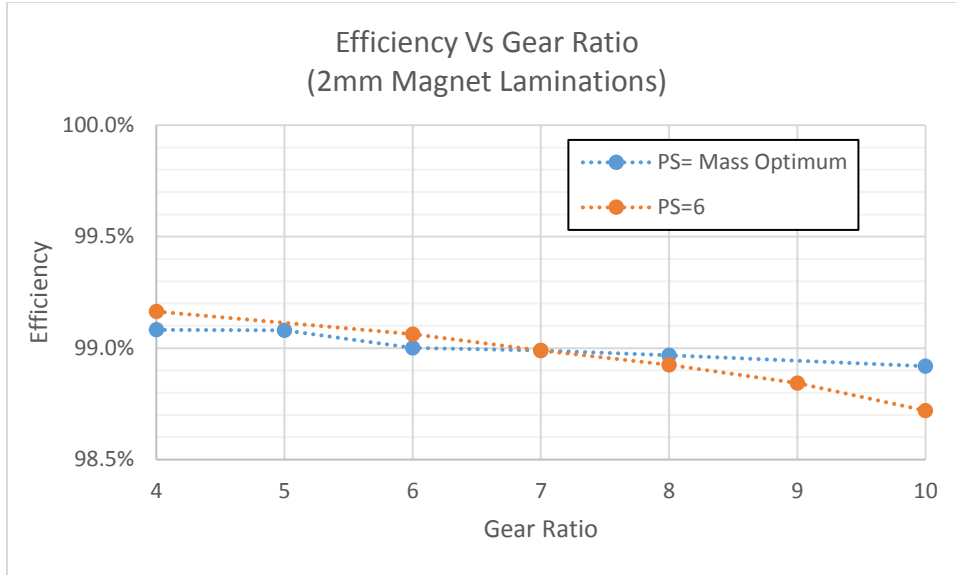
17

Figure 18 Effect of gear ratio on efficiency with 2 mm magnet laminations

IX. Effect of Radius

For the study of radius constant MS and MR values of 10 and 6 were again used. Parametric sweeps of radius, gear ratio, and PS were used to produce mass optimum gear designs. In order to account for mechanical tolerance considerations as radius increases, instead of holding a fixed airgap size, the mechanical airgap was defined by

$$ag = .0047 * D + .27 \tag{7}$$

where ag is mechanical airgap in mm and D is the diameter of a given rotor in mm. (Ref 26)

It is important to note that the results of this study do not account for the effects of 3D flux leakage, which have been shown to increase with increased gear radius (Ref 27). The trends presented are therefore only applicable as long as a reasonable axial length is maintained as radius is increased. Higher-level variable values used in this study are listed in Table 6.

Table 6 Values of higher-level variables used in radius study

Radius Study Parameters	
Radius (cm)	7, 8.75, 10.5, 12.25, 14
Gear Ratio	4,6,8,10
Sun Gear Pole Pairs (PS)	4-16
Magnets per Sun Gear Pole Pair (MS)	10
Magnets per Ring Gear Pole Pair (MR)	6
Mechanical Airgap (mm)	.0047*2*Radius+.27

D. Achievable 2D Electromagnetic Specific Torque

The variation of achievable specific torque with radius at various gear ratios is shown in Figure 19. The expectation would be that specific torque would increase significantly with increased gear radius. The plot, however, shows small improvements in specific torque when radius is increased at smaller radii, and a decrease in specific torque as radius is increased at larger radii. This discrepancy between the expectation and the plot results from significant increases to magnetic airgap between the sun gear and the modulator as radius and gear ratio increase. This significant magnetic airgap increase is caused by the mechanical airgap assumption of Equation 7 and increases to the required thickness of the sun magnet retaining hoop. Increasing either radius or gear ratio, increases the tip speed of the sun gear in these studies, because output speed is held fixed at 4000 rpm. Correspondingly, centripetal loading of the sun magnet

retaining hoop increases and additional carbon fiber hoop thickness is needed to retain the sun gear's magnets. The growth of the magnetic gap between the sun gear and modulator increases the reluctance of the coupling path in the gear and reduces the magnetic components ability to produce torque.
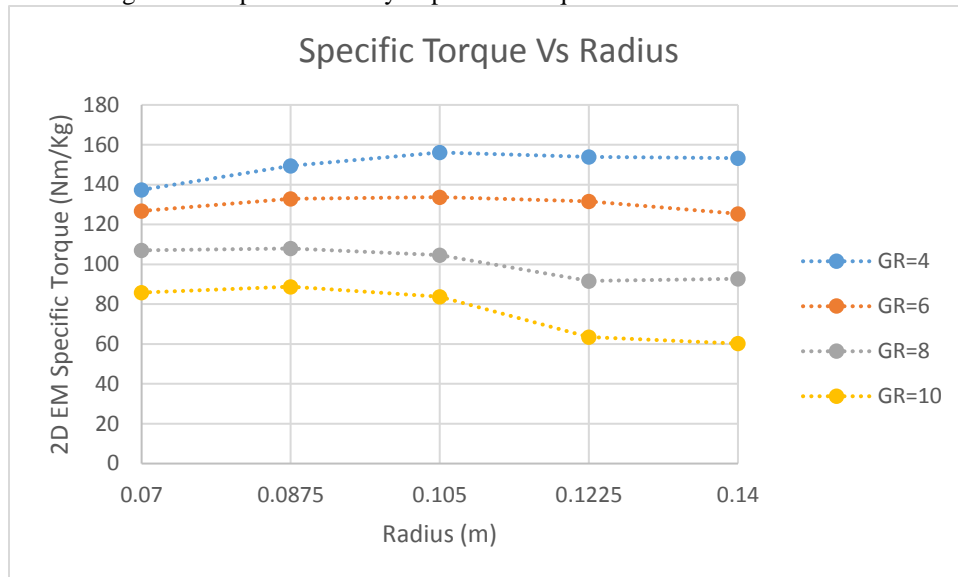

Figure 19 Effect of radius on achievable specific torque at various gear ratios

In order to illustrate more generally the variation in CMG specific torque with radius, the parametric sweeps used to produce Figure 19 were re-run without the carbon fiber hoop assumption. Equation 7 was still used to set the mechanical gap between the magnetic components. Figure 20 shows the results of that parametric sweep. Essentially, the results in Figure 20 represent the variation in specific torque with radius and gear ratio when the speed of the sun gear is low enough that a carbon fiber hoop is not required for sun magnet containment. The results show a significant increase in specific torque with radius resulting from the magnetic components being given a mechanical advantage.
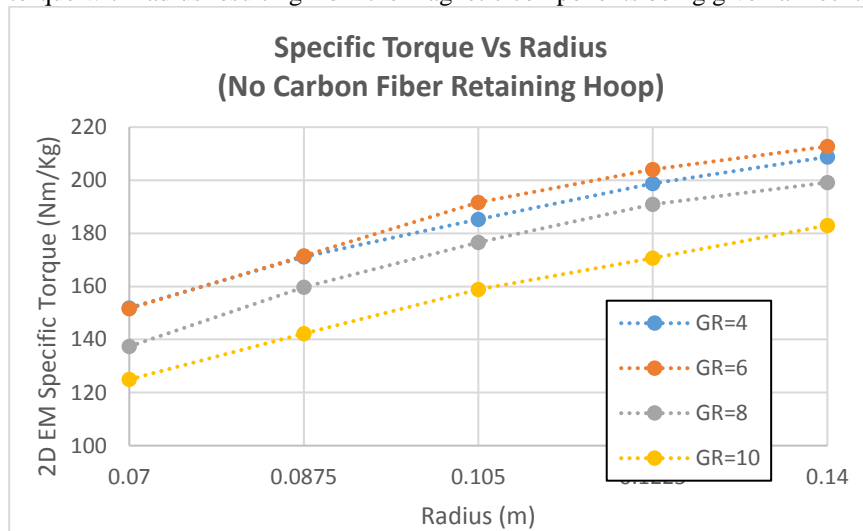

Figure 20 Effect of radius on specific torque when a sun magnet retaining hoop is not required.
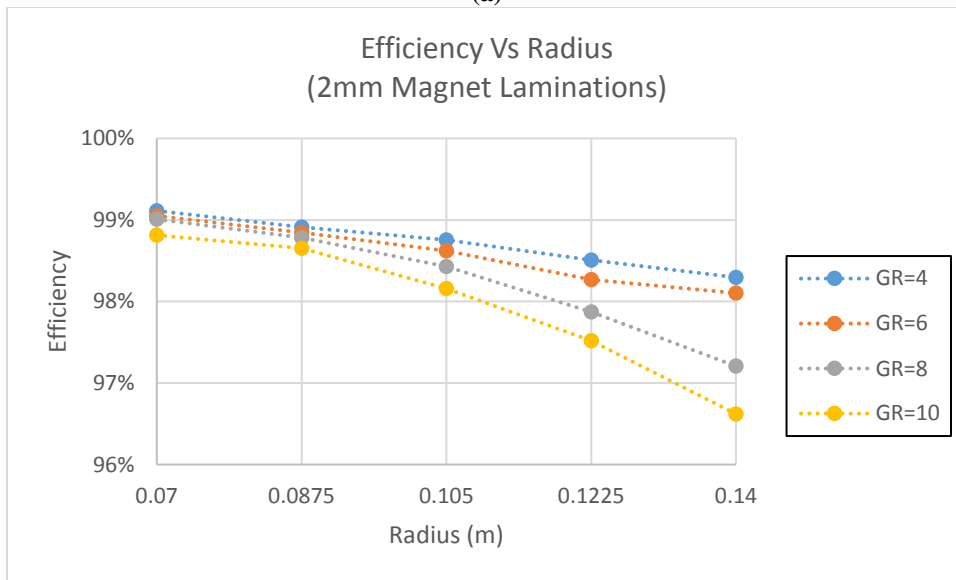
E. Efficiency Vs Radius

The effect of radius on magnetic gear efficiency is shown in Figure 21 both magnet lamination cases at the mass optimum PS values for each combination of gear ratio and radius. In both cases, with and without 2 mm magnet laminations, efficiency decays with increased radius.

Initially, as radius increases, optimum PS increases and mass decays (specific torque increases) as seen in Figure 18. The increasing PS, at a constant gear ratio, results in increased electrical frequency of all three rotors on one

another. The increased frequency results in increased losses even though gear mass is decreasing. At some point, as radius continues to increase, the increase in sun-to-modulator magnetic airgap causes the optimum PS value to become more constant with increased radius and mass begins to increase. The increasing mass causes further decay of gear efficiency. Without magnet laminations, increasing magnet width with increased radius also plays a significant role in the efficiency reduction with radius shown in Figure 21a.
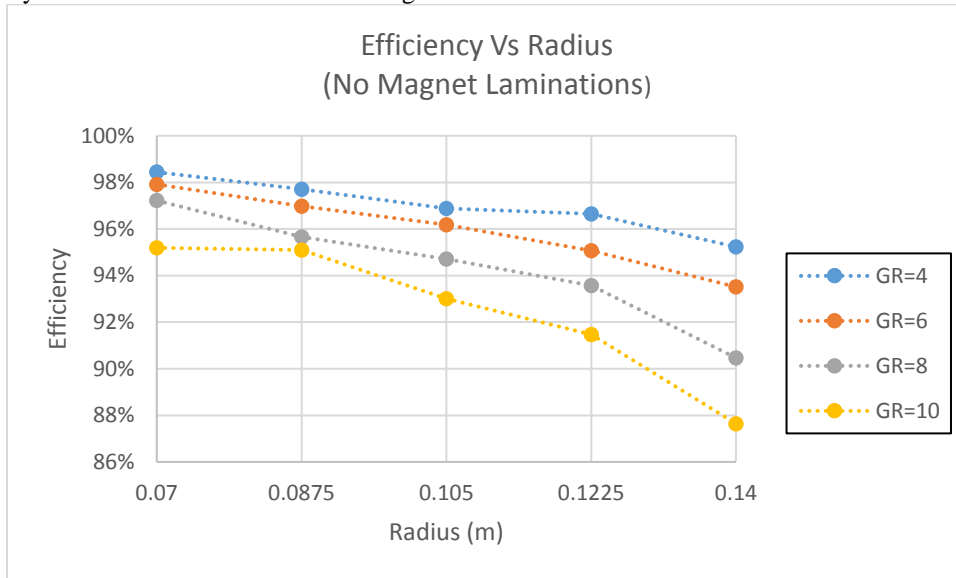
(a)

(b)

Figure 21 Effect of radius on efficiency. Mass-optimum PS value was used for each combination of gear ratio and radius

X.   Mass Vs Efficiency

Efficiency versus mass for all of the gear designs produced in the radius study of Section IX, with and without 2 mm magnet laminations, is plotted in Figure 22. Without 2 mm magnet laminations, a coupling between mass and efficiency can be seen in Figure 22a. This coupling appears because efficiency, in the absence of magnet laminations, is highly dependent on sun and ring gear magnet losses which are highly coupled to the mass and geometry of the magnets in the gear through Equation 3. Higher magnet per pole counts or magnet laminations can be used to remove this coupling as the plot with 2 mm magnet laminations in Figure 22b shows.
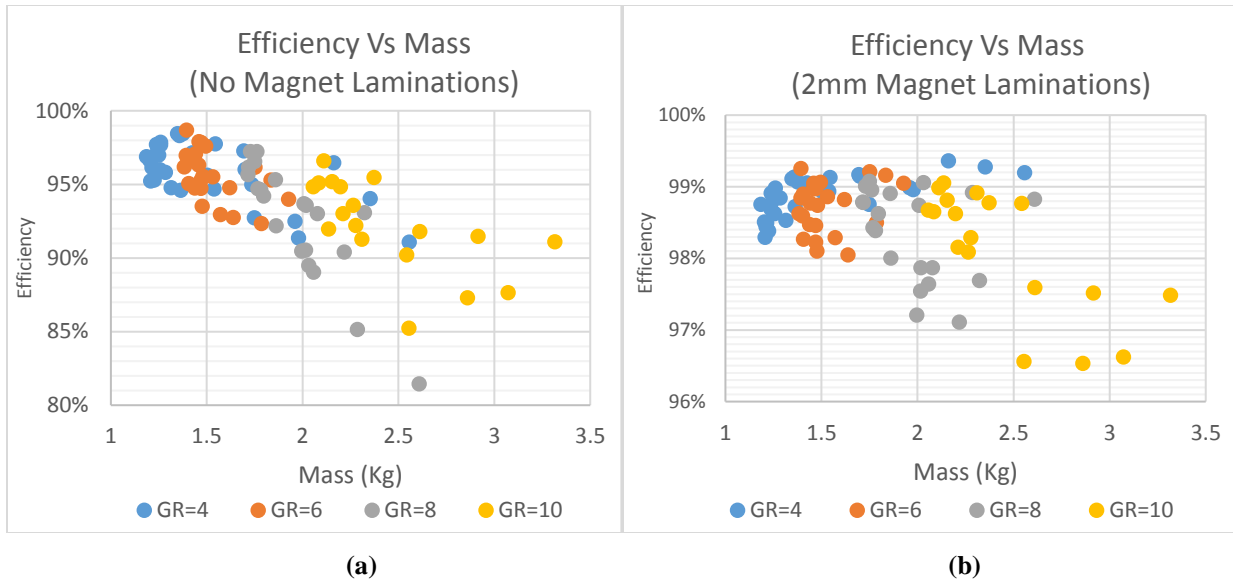
(a)   **(b)**

Figure 22 Efficiency trends with respect to mass for magnetic gears with and without laminated magnets.

With laminations there is less of a dependence of efficiency on the mass of the gear designs, because magnet losses are small and modulator iron loss is the predominate loss in the gears. Modulator iron loss is driven mostly by the magnetic flux from the sun gear and is therefore heavily coupled to the electrical frequency of the field the sun gear produces on the modulator's pole pieces. Figure 23 shows the same efficiency and mass data shown in Figure 22b plotted against electrical frequency. Gear efficiency is shown to decrease in an almost linear fashion with increased sun gear electrical frequency in Figure 23a, whereas there appears to be a mass optimizing sun gear electrical frequency around 3,000 Hz in Figure 23b.
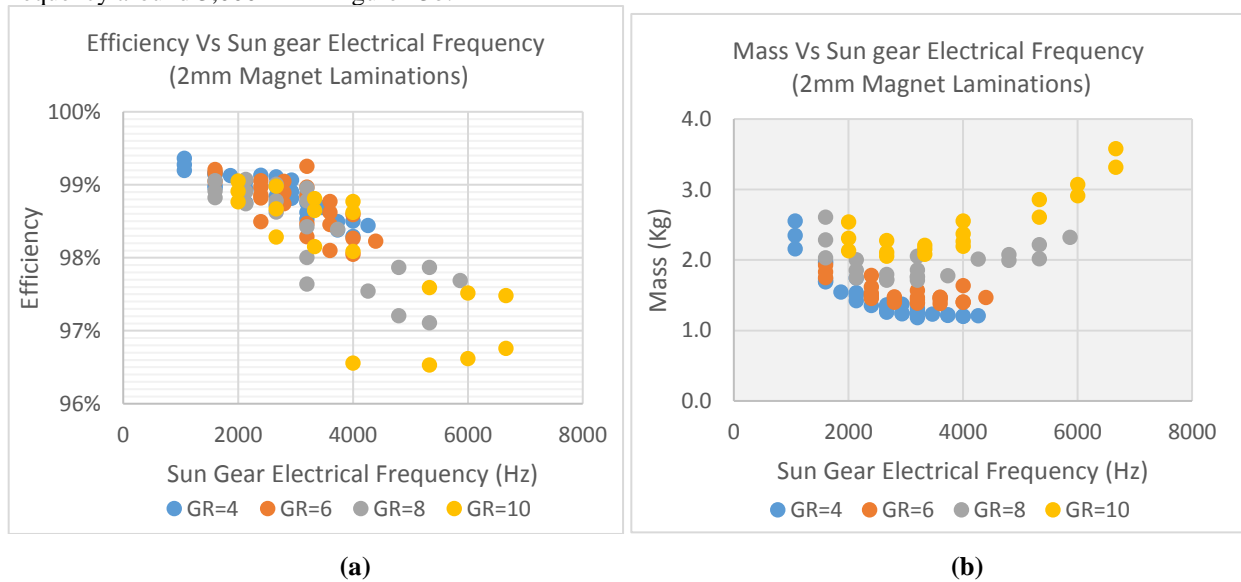

(a)   **(b)**

Figure 23 Effect of sun gear electrical frequency on magnetic gear specific torque with 2 mm magnet laminations

XI. Conclusion

This paper presented electromagnetic efficiency and 2D specific torque trends for concentric magnetic gears with respect to magnets per ring gear pole pair, magnets per sun gear pole pair, sun gear pole pairs, gear ratio, and radius. The data for these trends were created by mass optimizing gears for values of the parameters listed and then running efficiency studies on the mass-optimized gears. The lessons learned from these studies are:

1. Magnets per pole pair in a Halbach array on either the sun or ring gear improve concentric magnetic gear specific torque, until significant magnetic fill percentage is lost due to mechanical and manufacturing considerations. If 100% magnet fill can always be maintained with increased magnet per pole count, specific torque will always go up with increased magnets per pole count, but with diminishing marginal returns.
2. High magnet per pole pair count can significantly reduce the eddy current losses in a magnetic gear and may be an alternative to magnet laminations for enabling high efficiency.
3. At a given radius, gear ratio, and airgap size, there is an optimum number of sun gear pole pairs for maximizing specific torque. This optimum number is driven by limits on ring gear pole pair count that result from pole-to-pole flux leakage and magnetic fill percentage loss effects.
4. In the absence of magnet laminations, sun gear losses are the dominate losses in a magnetic gear. Sun gear losses trend heavily with the dimensions and thereby the mass of the sun gear magnets. Correspondingly efficiency trends with the mass of the gear.
5. In the presence of magnet laminations, modulator/iron loss is the dominate loss in a magnetic gear. Modulator loss trends with the electrical frequency of the sun and ring gear on the modulator. Correspondingly, efficiency trends with the electrical frequency of the sun and ring gear on the modulator.
6. Due to the high speed of the output assumed in this study, the required carbon fiber hoop thickness to retain the sun gear magnets greatly increased the magnetic airgap between the sun gear and modulator as radius and/or gear ratio increased. The larger magnetic airgaps resulted in specific torque decaying with gear ratio and limited specific torque increases with radius.
7. At speeds where a carbon fiber hoop is not required to retain the sun magnets, magnetic gear specific torque increases nearly linearly with radius.

XII.   Appendix

A. Magnet Eddy Current Model

Eddy currents in the magnets were predicted using the eddy current model for general periodic waves found in Reference 24. The model defines volumetric loss in a component experiencing a periodically varying magnetic field as

$$P_c = \frac{1}{16}\frac{V}{\rho}\frac{w^2 l^2}{w^2 + l}\frac{1}{T}\int_0^T (\frac{dB}{dt})^2\, dt$$

Where P_c is the volumetric loss, w the tangential thickness of the magnet, l is the axial length of a given magnet section, V is the volume of the magnet, ρ is the resistivity of the material, T is the period of repetition, and B is magnetic field magnitude.

Using numerical integration this equation can be written

$$P_c = \frac{1}{16}\frac{V}{\rho}\frac{w^2 l^2}{w^2 + l}\frac{1}{\Delta t * N}\sum_{i=1}^{N}(\frac{\Delta B_i}{\Delta t_i})^2\, \Delta t_i$$

Where N is the number of time steps and Δt is the length of the time step. Because Δt is constant this equation can be simplified to

$$P_c = \frac{1}{\Delta t^2}\frac{1}{16}\frac{V}{\rho}\frac{w^2 l^2}{w^2 + l}\frac{1}{N}\sum_{i=1}^{N}\Delta B_i{}^2$$

B. Pole Piece Iron Loss Model

Modulator loss was predicted using the Improved Generalized Stienmetz Equation (IGSE) with minor loop separation method found in Reference 25. The IGSE is a modification to the Stienmetz Equation that allows for accurate prediction of core loss when the magnetic field is not sinusoidal. The Stienmetz Equation defines the specific core loss (loss per Kg of material) in electrical steel subjected to a sinusoidal varying magnetic field as

$$P_v = k * f^\alpha B^\beta$$

Where P_v is specific core loss, f is the frequency of the sinusoidal varying magnetic field, B is the peak value of the field, and k, α, and β are material constants. k, α, and β can generally be determined from core loss information

provided by electrical steel manufacturers. The IGSE uses these parameters to predict core loss for non-sinusoidal waves as

$$P_v = \frac{1}{T} \int_0^T k_1 \left| \frac{dB}{dt} \right|^\alpha (\Delta B)^{\beta - \alpha} dt$$

$$k_1 = \frac{k}{2^{\beta - 1} \pi^{\alpha - 1} \int_0^{2\pi} |\cos(\theta)|^\alpha d\theta}$$

Where T is the period of repetition of the field, ΔB is the peak to peak flux density, and k_1 is an updated loss coefficient. The algorithm for numerically implementing this equation with minor loop separation is discussed in detail in Reference 25. This algorithm was implemented on the magnetic field vs rotor position data from the finite element simulation. By a similar method as used for the magnet loss, modulator loss can also be written

$$Loss_{mod} = C_{mod} * \frac{1}{\Delta t}^\alpha$$

Where $Loss_{mod}$ is the modulator losses and C_{mod} is the modulator loss coefficient.

This loss prediction is only meant to serve as a min baseline for modulator loss in the gear as the IGSE most likely under predicts the losses. The IGSE is only accurate for unidirectional fields and therefore it doesn't account for the losses from the rotating fields (Ref 28). Iron loss is the most likely location that additionally losses need to be added based on the thermal behavior and efficiency testing of the gear

XIII. Acknowledgments

XIV. References

1. Anderson, A.D., Renner, N.J., Wang, Y., Lee, D., Agrawal, S., Sirimanna, S., Haran, K., Banerjee, A., Starr, M., and Felder, J., "System Weight Comparison of Electric Machine Topologies for Electric Aircraft Propulsion" 2018 AIAA/IEEE Electric Aircraft Technologies Symposium. Cincinnati, Ohio.

2. Zhang, X., Bowman, C. L., O'Connell, T. C., and Haran, K. S., "Large electric machines for aircraft electric propulsion," IET Electric Power Applications, vol. 12, issue 6, 2018.

3. Borisavljevic, A., "Limits, Modeling, and Design of High-Speed Permanent Magnet Machnines," ISBN 978-3-642-33457-3, Springer 2013

4. Astridge, D., and Savage, M., "Rotorcraft Drivetrain Life Safety and Reliability," AGARD Report No. 775, North Atlantic Treaty Organization Advisory Group For Aerospace Research And Development, June 1990

5. Zaretsky, E. V., "Bearing and Gear Steels for Aerospace Applications" NASA Technical Memorandum 102529, NASA, March 1990

6. Desvaux, M., Bildstein, H., Sire, S., and Fasquelle, A., "Magnetic Losses and Thermal Analysis in a Magnetic Gear for Wind Turbine," 13th International Conference on Ecological Vehicles and Renewable Energies, IEEE, 2018

7. Johnson, M., Gardner, M.C., Toliyat, H. A., Englebretson, S., Ouyan, W., and Tschida, C., "Design, Construction, and Analysis of a Large-Scale Inner Stator Radial Flux Magnetically Geared Generator for Wave Energy Conversion," IEEE Transactions on Industrial Applications Vol 50 No 4, July/August 2018

8. McGilton, B., Crozier, R., McDonal, A., and Mueller, M., "Review of Magnetic Gear Technologies and Their Applications in Marine Energy," IET Renewable Power Generation Conference, IET, December 2017

9. Frandsen, T.v., Rasmussen P.O., and Jensen K.K., "Improved Motor Integrated Permanent Magnet Gear for Traction Applications," 2012 IEEE Energy Conversion Congress and Exposition (ECCE)

10. Jian, L., Chau, K.T., and Jian, J.Z., " An Integrated Magnetic-Geared Permanent-Magnet In-Wheel Motor Drive for Electric Vehicles," IEEE Vehicle Power and Propulsion Conference, IEE, September 3-5, 2008

11. Jansen, R., Brown, G. V., Felder, J. L., and Duffy, K. P., "Turboelectric Aircraft Drive Key Performance Parameters and Functional Requirements," American Institute of Aeronautics and Astronautics, 2015

12. Kirsten P. Duffy and Ralph Jansen. "Partially Turboelectric and Hybrid Electric Aircraft Drive Key Performance Parameters", 2018 AIAA/IEEE Electric Aircraft Technologies Symposium, AIAA Propulsion and Energy Forum, (AIAA 2018-5023)

13. Asnani, V., Scheidler, J., and Tallerico, T., "Magnetic gearing research at NASA," Proc. of AHS Int. 74th Annual Forum, Phoenix, AZ, May 14-17, 2018.

14. Scheidler, J. J., Asnani, V. M., and Tallerico, T. F., "NASA's magnetic gearing research for electrified aircraft propulsion," Proc. of AIAA/IEEE Electric Aircraft Technologies Symposium, Cincinnati, OH, Aug 21-22, 2018.

15. Scheidler, J.J., Cameron, Z. A., and Tallerico, T. F., "Dynamic Testing of a High Specific Torque Concentric Magnetic Gear," Proc. of the Vertical Flight Society's 75th Annual Forum, Philadelphia, PA, May 13-16, 2019

16. Cameron, Z. A., Tallerico, T. F, and Scheidler, J.J. "Lessons Learned in Fabrication of a High-Specific-Torque Magnetic Gear," Proc. of the Vertical Flight Society's 75th Annual Forum, Philadelphia, PA, May 13-16, 2019

17. Gardner, M.C., Johnson, M., and Toliyat, H. A., "Comparison of Surface Permanent Magnet Axial and Radial Flux Coaxial Magnetic Gears," IEEE Transactions on Energy Conversion, 2018

18. Johnson, M., Gardner, M.C., and Toliyat, H. A., "Design Comparison of NbFeB and Ferrite Radial Flux Surface Permanent Magnet Coaxial Magnetic Gears," IEEE Transactions on Industrial Applications Volume 54 Issue 2, IEEE, October 2017

19. Johnson, M., Gardner, M.C., and Toliyat, H. A., "Analysis of High Gear Ratio Capabilities for Single-Stage, Series Multistage, and Compound Differential Coaxial Magnetic Gears," in IEEE Transactions on Energy Conversion, vol. 34, no. 2, pp. 665-672, June 2019.

20. Li, X., Chau, K. T., Cheng, M., and Hau, W., "Comparison of Magnetic Geared Permanent Magnet Machines" Progress in Electromagnetics Research Vol 133 pg 177-198, 2013

21. Atallah, K., Calverley, S., and Howe, D., "Design, analysis and realization of a high-performance magnetic gear," Proc. of IEEE Electric Power Applications, p. 135-143, 2004.

22. Zhu, Z.Q., and Howe, D.: 'Influence of design parameters on cogging torque in permanent magnet machines', IEEE Trans. Magn., 2000, 15, (5), pp. 407–412

23. Jungmayr, G., Loeffler, J., Winter, B., Jeske, F., and Amrhein, W., "Magnetic gear: radial force, cogging torque, skewing, and optimization," IEEE Transactions on Industry Applications, p. 3822-3830, 2016.

24. Rouho, S., Santa-Nokki, T., Kolehmainen, J., and Arkkio, A., "Modeling Magnet Length in 2-D Finite Element Analysis of Electric Machine," IEEE Transactions on Magnetic Vol 45 No 8, IEEE, August 2009

25. K. Venkatachalam, C. Sullivan, T. Abdallah, and H. Tacca, "Accurate prediction of ferrite core loss with non-sinusoidal waveforms using only Steinmetz parameters," in Computers in Power Electronics, 2002. Proceedings. 2002 IEEE Workshop on, June 2002, pp. 36 – 41

26. Duan, Y. and Ionel, D.M., "Nonlinear Scaling Rules for Brushless PM Synchronous Machines Based on Optimal Design Studies for a Wide Range of Power Ratings," in IEEE Transactions on Industry Applications, vol. 50, no. 2, pp. 1044-1052, March-April 2014.

27. Gerber, S. and Wang, R-J., "Analysis of the end-effects in magnetic gears and magnetically geared machines," 2014 International Conference on Electrical Machines Proceedings, Berlin, German, pp. 396 – 402, Nov. 2014.

28. Krings, "Iron Losses in electrical Machines – Influence of Material Properties, Manufacturing Processes, and Inverter Operation" Doctoral Thesis KTH University. Stockholm, Sweden 2014